The Astrophysical Journal, 658:829–839, 2007 April 1

CHEMICAL ABUNDANCES IN AN AGN ENVIRONMENT: X-RAY/UV CAMPAIGN ON THE MARKARIAN 279 OUTFLOW[1]

Nahum Arav,[2] Jack R. Gabel,[3] Kirk T. Korista,[4] Jelle S. Kaastra,[5] Gerard A. Kriss,[6,7] Ehud Behar,[8] Elisa Costantini,[5,9] C. Martin Gaskell,[10] Ari Laor,[8] C. Nalaka Kodituwakku,[4] Daniel Proga,[11] Masao Sako,[12] Jennifer E. Scott,[13] and Katrien C. Steenbrugge[14]

Received 2006 July 20; accepted 2006 November 28

ABSTRACT

We present the first reliable determination of chemical abundances in an active galactic nucleus (AGN) outflow. The abundances are extracted from the deep and simultaneous *Far Ultraviolet Spectroscopic Explorer* (*FUSE*) and *Hubble Space Telescope* (*HST*) STIS observations of Mrk 279. This data set is exceptional for its high signal-to-noise ratio, unblended doublet troughs, and little Galactic absorption contamination. These attributes allow us to solve for the velocity-dependent covering fraction and therefore obtain reliable column densities for many ionic species. For the first time, we have enough such column densities to simultaneously determine the ionization equilibrium and abundances in the flow. Our analysis uses the full spectral information embedded in these high-resolution data. Slicing a given trough into many independent outflow elements yields the extra constraints needed for a physically meaningful abundance determination. We find that relative to solar, the abundances in the Mrk 279 outflow are (linear scaling) carbon 2.2 ± 0.7, nitrogen 3.5 ± 1.1, and oxygen 1.6 ± 0.8. Our UV-based photoionization and abundance results are in good agreement with the independent analysis of the simultaneous Mrk 279 X-ray spectra. This is the best agreement between the UV and X-ray analyses of the same outflow to date.

Subject headings: galaxies: abundances — galaxies: active — galaxies: individual (Mrk 279) — galaxies: Seyfert — line: formation — quasars: absorption lines

1. INTRODUCTION

Active galactic nuclei (AGNs) provide a vital probe of the early history of chemical enrichment in the universe (Shields 1976; Hamann & Ferland 1992; Ferland et al. 1996; Dietrich et al. 2003). Their brightness allows us to see chemically processed environments when the universe was less than 7% of its current age (Fan et al. 2004), thus giving us insights into early star formation and galaxy evolution. The spectra of the highest redshift AGNs are very similar to those of AGNs in the local universe (Fan et al. 2004), suggesting that chemical enrichment of their environments operates on short cosmological timescales. This feature makes local AGNs a good probe of chemical processing in the early universe.

There are two main tracks for determining abundances in AGNs: broad emission lines (BELs) are seen in most AGNs and are known to be formed in close proximity to the nucleus (within 0.01–0.1 pc.; Kaspi et al. 2005, and references therein). Considerable effort has been devoted to determining abundances in AGNs by studying the relative strength of BELs in individual as well as composite spectra (e.g., Shields 1976; Baldwin & Netzer 1978; Hamann & Ferland 1992; Ferland et al. 1996; Dietrich et al. 1999, 2003). These studies suggest that the metallicity of the BEL region (BELR) is supersolar. However, BEL abundance studies are only relative, in the sense that they do not measure the ratio of heavy elements to hydrogen directly. Ratios of nitrogen to carbon and oxygen BELs are measured and then converted to metallicity (Z) using the expected secondary nucleosynthesis of nitrogen, which predicts N/O and N/C $\propto Z$ or N/H $\propto Z^2$ (Hamann & Ferland 1999). This assumption weakens the robustness of the BEL metallicity claims in principle. In the best case, where H I measurements of galactic environment are available in a high-redshift galaxy, this assumption is not verified (Pettini et al. 2002). Furthermore, there are considerable systematic issues that affect these studies. The BELR is spatially stratified and likely to have a wide range of densities and temperatures (Nagao et al. 2006). Therefore, different BELs can arise from largely different regions, which complicates the use of BEL line-flux ratios as abundance indicators. Radiation transfer inside the opaque BEL material is a difficult problem that further complicates interpreting observed BEL ratios (Netzer 1990).

The second track for determining abundances is using absorption lines associated with AGN outflows. In principle, absorption-line studies allow for absolute abundance measurements, since the

[1] Based on observations made with the NASA/ESA *Hubble Space Telescope* and the NASA-CNES-CSA *Far Ultraviolet Spectroscopic Explorer*, and obtained at the Space Telescope Science Institute, which is operated by the Association of Universities for Research in Astronomy, Inc., under NASA contract NAS 5-26555.

[2] Center for Astrophysics and Space Astronomy, University of Colorado, Boulder, CO 80309-0389; arav@colorado.edu.

[3] Department of Physics, Creighton University, Omaha, NE 68178; JackGabel@creighton.edu.

[4] Department of Physics, Western Michigan University, Kalamazoo, MI 49008; korista@wmich.edu.

[5] SRON National Institute for Space Research, 3584 CA Utrecht, Netherlands; J.S.Kaastra@sron.nl, e.costantini@sron.nl, K.C.Steenbrugge@sron.nl.

[6] Space Telescope Science Institute, Baltimore, MD 21218; gak@stsci.edu.

[7] Center for Astrophysical Sciences, Department of Physics and Astronomy, The Johns Hopkins University, Baltimore, MD 21218.

[8] Department of Physics, Technion, Haifa 32000, Israel; behar@physics.technion.ac.il, laor@physics.technion.ac.il.

[9] Astronomical Institute, University of Utrecht, 3508 TA Utrecht, Netherlands.

[10] Department of Physics and Astronomy, University of Nebraska, Lincoln, NE 68588-0111; mgaskell1@unl.edu.

[11] Physics Department, University of Nevada, Las Vegas, NV 89154-4002; dproga@physics.unlv.edu.

[12] Department of Physics and Astronomy, University of Pennsylvania, Philadelphia, PA 19104; masao@sas.upenn.edu.

[13] Department of Physics, Astronomy, and Geosciences, Towson University, Towson, MD; jescott@towson.edu.

[14] Department of Physics, University of Oxford, Oxford, OX1 3RH, UK; kcs@astro.ox.ac.uk.

hydrogen Lyman series troughs can yield direct ratios of hydrogen to heavy elements. AGN outflows are evident by resonance line absorption troughs, which are blueshifted with respect to the systemic redshift of their emission counterparts. In Seyfert galaxies, velocities of several hundred km s^{-1} (Crenshaw et al. 1999; Kriss et al. 2000) are typically observed in both UV resonance lines (e.g., C IV $\lambda\lambda$1548.20, 1550.77, N V $\lambda\lambda$1238.82, 1242.80, O VI $\lambda\lambda$1031.93, 1037.62, and Lyα), as well as in X-ray resonance lines (Kaastra et al. 2000, 2002; Kaspi et al. 2000, 2002). Similar outflows (often with significantly higher velocities) are seen in quasars, which are the luminous relatives of Seyfert galaxies (Weymann et al. 1991; Korista et al. 1993; Arav et al. 2001a). Distances of the outflows from the central source can range from smaller than BELR distances (QSO 1603+3002; Arav et al. 1999a) to tens of parsecs (NGC 3783; Gabel et al. 2005b) or 1000 pc (QSO 1044+3656; de Kool et al. 2001). Thus, in most cases, the outflows are associated with material in the vicinity of the AGN and can be used as diagnostics for the chemically enriched environment at the center of galaxies.

A main obstacle in determining abundances using outflow absorption lines is obtaining reliable measurements of the absorption column densities from the troughs. In the last few years, our group (Arav 1997; Arav et al. 1999a, 1999b, 2002, 2003; de Kool et al. 2001) and others (Barlow 1997; Telfer et al. 1998; Churchill et al. 1999; Ganguly et al. 1999) have shown that in quasar outflows, most lines are saturated even when not black. As a consequence, the apparent optical depth method, which stipulates that the optical depth $\tau_{ap} \equiv -\ln(I)$, where I is the residual intensity in the trough, is not a good approximation for outflow troughs. In addition, using the doublet method (Barlow 1997; Hamann et al. 1997), we have shown that in many cases the shapes of the troughs are almost entirely due to changes in the line-of-sight covering as a function of velocity, rather than to differences in optical depth (Arav et al. 1999a, 2001a; de Kool et al. 2001; Gabel et al. 2005a). Gabel et al. (2003) show the same effect in the outflow troughs of NGC 3783, as does Scott et al. (2004) for Mrk 279. As a consequence, the column densities inferred from the depths of the troughs are only lower limits.

In order to measure reliable column densities, we found it necessary to use a two-step combination: first, we developed analysis methods that can disentangle the covering factors from the optical depth (Gabel et al. 2003, 2005a). Second, these methods depend on having high-resolution ($\gtrsim$20,000) and high signal-to-noise (S/N $\gtrsim$ 20) spectral data of outflow troughs. Furthermore, we critically rely on fully resolved uncontaminated doublet and multiple troughs. Mrk 279 is the optimal target for such analysis, since it allows us to obtain data with the above specification on the C IV, N V, and O VI doublets, as well as on several Lyman series troughs. The latter are crucial for any abundance determination (see § 5.1). Before applying this analysis to the Mrk 279 data, we tested the validity of our absorption model. The main alternatives are inhomogeneous absorber models (de Kool et al. 2002). We tested the main variants of inhomogeneous absorber models on the Mrk 279 data set and concluded that the outflow cannot be fitted well with these models (Arav et al. 2005; see § 5.2.1). Following these tests, we used the partial covering absorber model to extract the column densities of all the observed ions in the Mrk 279 outflow (Gabel et al. 2005a).

In this paper we present the determination of chemical abundances in the AGN outflow emanating from Mrk 279, using the high-quality simultaneous UV data sets from *HST*/STIS and *FUSE*. Our procedure for determining the abundances is as follows. First, we treat each spectral resolution element as an independent measurement (see § 5.1 for discussion). After determining the spectral energy distribution (SED) appropriate for Mrk 279 (§ 2.2), we solve for the ionization parameter (U) and the total hydrogen column density (N_H) independently for each of our 15 resolution elements (§ 2.3). This is done by comparing the measured column densities with photoionization grid models, assuming a given set of CNO abundances. Each resolution element is allowed to have a different combination of U and N_H. However, we require the same set of CNO abundances for all resolution elements. The CNO composition of the outflow is determined to be the abundance set that yields the best fit for all 15 resolution elements (§ 3). Section 4 is devoted to a comparison of the photoionization and abundance results presented here with the independent analysis of the simultaneous Mrk 279 X-ray spectra. In § 5 we discuss our results. The Appendix gives the details for the extraction of ionic column densities from the observed troughs, with emphasis on the associated errors.

2. PHOTOIONIZATION ANALYSIS

2.1. *The Mrk 279 Data Set*

In May 2003 we obtained simultaneous X-ray and UV observations of the Mrk 279 AGN outflow (description of the UV observations is found in Gabel et al. [2005a] and of the X-ray observations in Costantini et al. [2006]). The 92 ks *FUSE* data have a spectral resolution of 20,000 and cover the observed wavelength 905–1187 Å. These data yielded the highest quality O VI trough spectrum of any AGN outflow to date. The 16 orbit *HST*/STIS/E140M observations have a spectral resolution of 40,000 and cover the observed wavelength 1150–1730 Å. These data yielded high-quality C IV and N V troughs. The combined *HST*/*FUSE* spectrum gives high signal-to-noise Lyα, Lyβ, and Lyγ troughs. Compared with other well-studied AGN outflow targets, the Galactic H I column density in the direction of Mrk 279 is quite low: 1.6 compared with 4.4 and 8.7 for Mrk 509 and NGC 3783, respectively (in units of 10^{20} cm^{-2}; Hwang & Bowyer 1997; Kaspi et al. 2002). Therefore, the outflow troughs of Mrk 279 are significantly less contaminated with Galactic absorption features than the other noted targets.

In Gabel et al. (2005a), we used a global fitting technique to extract three velocity-dependent quantities from the data: continuum covering factor, BELR covering factor, and column densities N_{ion} for all the detected ions. An important finding was that the outflow fully covers the continuum both for the Lyman series troughs and for the CNO doublets. In this paper, we refine the N_{ion} measurements by using this finding. Once the continuum coverage is known to be 100%, the doublet equations are reduced to two unknowns (BELR covering factor and optical depth), which we can solve independently for each ion, since we have two residual intensity equations. These solutions are more physical, and their errors are easier to estimate. In the Appendix, we give the details of the new solution, while for the rest of the paper, we use this improved set of N_{ion} determinations. The difference between the Gabel et al. (2005a) and the current N_{ion} measurements can be seen in the first figure of the Appendix (Fig. 6). We point out that the main difference is in the size of the error bars, where we put much effort into obtaining physically accurate errors, since the analysis is crucially dependent on these.

2.2. *Photoionization Modeling and SED*

We use simple slab photoionization models (using the code CLOUDY; Ferland 1998). Such models are commonly used in the study of quasar outflows (e.g., Weymann et al. 1985; Arav et al. 1994, 2001b; Hamann 1996; Crenshaw et al. 1999; Gabel et al. 2006) and assume that the absorber consists of a constant density

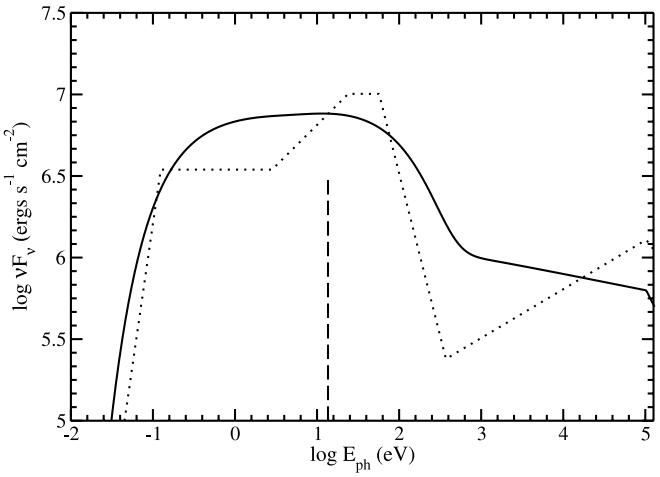

FIG. 1.—SED used for our analysis (*solid line*) compared with the canonical Mathews-Ferland spectrum. The two SEDs are normalized to the same flux at 1 ryd (*dashed line*; 1 ryd is equivalent to 13.6 eV or 912 Å). The Mrk 279 model incident SED was constructed to smoothly connect the *FUSE* spectrum near rest-frame 900 Å to the *Chandra*/LETGS spectrum near 200 eV (see text for details). Compared with the Mathews-Ferland SED, the Mrk 279 SED is somewhat harder.

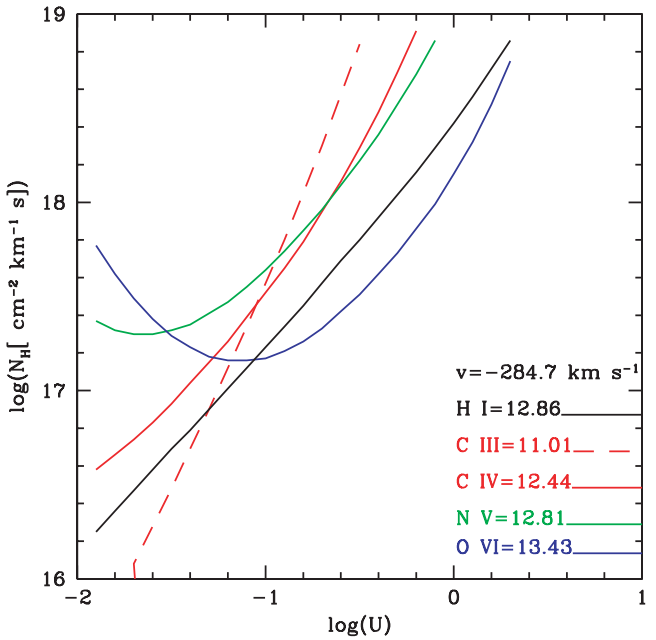

FIG. 2.—Curves of constant ionic column density plotted on the plane of total hydrogen column density (N_H) per unit velocity of the slab vs. the ionization parameter of the incident radiation (U), using solar abundances and an SED tailored for these specific observations of Mrk 279 (see Fig. 1). The inset key shows measured log (N_{ion}) (per unit velocity) for the resolution element centered around the -285 km s^{-1} outflow velocity.

slab irradiated by an ionizing continuum. The two main parameters in these models are the thickness of the slab, as measured by the total hydrogen column density (N_H), and the ionization parameter U (defined as the ratio of number densities between hydrogen ionizing photons and hydrogen in all forms).

The SED of the incident flux is also important in determining the ionization equilibrium. The ionizing SED of Mrk 279 is arguably the most tightly constrained of any AGN to date. *FUSE* observations set the flux at ~900 Å in the object's rest frame, and the *Chandra*/LETGS *simultaneously* provided reliable X-ray coverage for energies greater than 200 eV. Even so, some ambiguity remains due to the gap between 13.8 eV and 200 eV (see Fig. 1). We opted to continue the slope of the *FUSE* continuum and gradually steepen it until it matched the soft X-ray continuum. We chose this shape rather than connecting these two points with a simple power law, since we consider it unlikely that a spectral break falls immediately at the edge of the observed UV data. We note that the 13.8–200 eV continuum would be somewhat softer with a simple power law connecting the UV and X-ray data and elaborate on the ramifications of such an SED in the discussion (§ 5).

To generate the Mrk 279 SED shown in Figure 1, we used the CLOUDY `agn` command, which generates the sum of two continua, $F_\nu = A\nu^{\alpha_{uv}} \exp(-h\nu/kT_{uv}) + B\nu^{\alpha_x}$. The first of these represents the optical/UV bump, and this command also imposes a low-energy exponential cutoff at 1 μm. We chose $\alpha_{uv} = -1.0$ and $kT_{uv} = 136$ eV to smoothly and conservatively span the 900 Å-200 eV spectral region. The second of the continua represents a high-energy (X-ray) power law that lies between 1 ryd and 100 keV, with cutoffs at both ends. We chose a slope to match the observed one, $\alpha_x = -1.1$, and normalized this component's strength relative to the UV bump with an $\alpha_{ox} = -1.35$. The CLOUDY input command string that generated this continuum is `agn 6.2 -1.35 -1.0 -1.1`, where the first parameter is log T_{uv}, followed by α_{ox}, α_{uv}, and α_x.

2.3. *Velocity-Dependent Grid Models*

We base our photoionization analysis, and ultimately the abundance determinations, on the grid-of-models approach created by Arav et al. (2001b). For a given N_{ion}, we ran a grid of models spanning 3 orders of magnitude in both N_H and U. For these models, we use the Mrk 279 SED described above and assume solar abundances, as given by the CLOUDY code, where the carbon and oxygen abundances are taken from Allende Prieto et al. (2002, 2001), and the nitrogen abundance is taken from Holweger (2001). The solar abundances of these elements compared to hydrogen are $C = 2.45 \times 10^{-4}$, $N = 8.5 \times 10^{-5}$, and $O = 4.9 \times 10^{-4}$. We then determine which combinations of N_H and U reproduce the observed N_{ion} and plot the ion curve, which is the locus of these points on the N_H-U plane. We do that for each measured N_{ion}. Ideally, a single value of N_H and U should be able to reproduce all the N_{ion} constraints. This is based on the assumption that the measured N_{ion} arise from a parcel of gas with uniform density that is irradiated by the given SED. On the N_H-U plane, this single-value solution will be represented by the crossing of all the ion curves at a single point.

A new feature that adds considerable diagnostic power to these models is their velocity dependence. Since the N_{ion} measurements are for a specific velocity, we obtain a grid model for each element of resolution along the trough. There is no a priori reason why material flowing in different velocities should have the same ionization structure or have the same column density per unit velocity (see § 5.1). Separating the absorption trough into individual resolution elements therefore allows for a more accurate solution of the ionization structure of the flow, and as we show below, is the key for precise abundance determination.

Figure 2 shows the grid model for the resolution element centered around the -285 km s^{-1} outflow velocity. All the measured ions are represented. The upper limits from Si IV, S IV, S VI, and C II do not add meaningful constraints and are consistent with the results of our analysis. An important advantage over the analysis of the PG 0946+301 spectra (Arav et al. 2001b), is that all the N_{ion} shown in Figure 2 are actual measurements and not lower limits, as was the case for most ions in PG 0946+301.

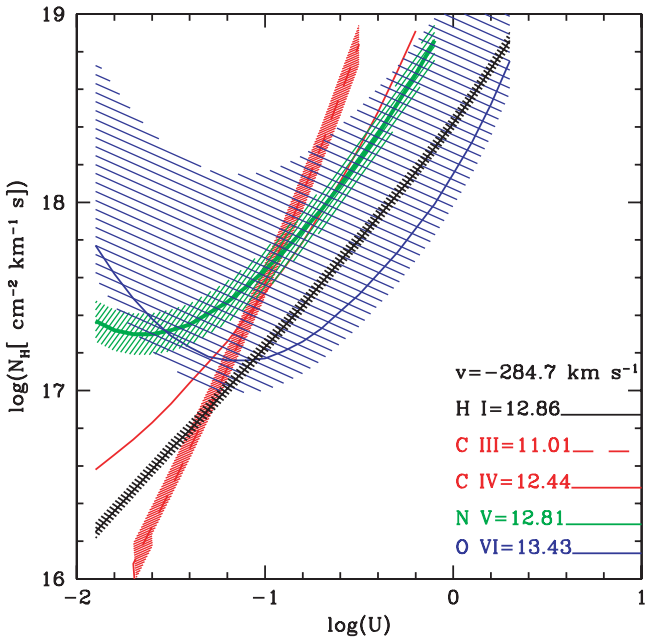

FIG. 3.—Same as Fig. 2, but including 1 σ uncertainties, shown as shaded areas with the same color as the associated ion curve. For the sake of clarity, we omitted the 1 σ presentation for C IV. As a figure of merit, in this velocity plot, the 1 σ interval for C IV touches the H I curve around $\log(U) = -1.4$.

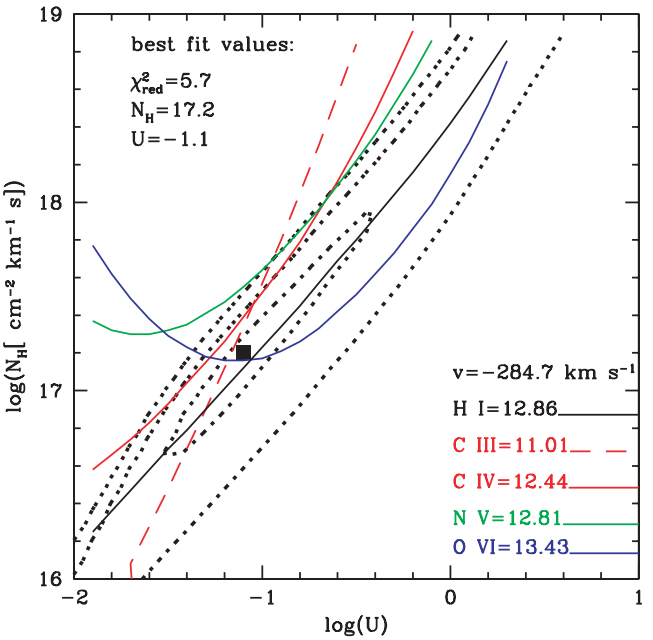

FIG. 4.—Similar to Fig. 2, but overplotted with reduced χ^2 contours (at 12.5, 50, and 112) for an N_H, U solution (*dotted lines*). Position of the formal solution is marked by the square, and the best-fit values are shown at the top left corner. From the large value of the reduced χ^2, it is evident that there is no acceptable N_H, U solution for this solar abundance model.

2.4. *Measurement Errors and χ^2 Analysis*

In measuring the N_{ion} for the outflow troughs in Mrk 279, we accounted for most of the systematic issues that plagued previous measurements. Unblended doublet and multiplet troughs were used, without which reliable outflow N_{ion} cannot be measured in principle. Both the continuum and BELR covering factors were taken into consideration, and N_{ion} as a function of velocity was extracted. We therefore possess the first comprehensive set of reliable N_{ion} measurements for an AGN outflow.

Extracting meaningful constraints on the ionization equilibrium and abundances from the measured N_{ion} requires having a reliable database of the associated errors. Estimating physical errors for the N_{ion} measurements is a complicated process that is fully described in the Appendix. Here we give a brief description of this process and a qualitative explanation for the different error values of the individual ions. For all ions except C III, the fitting procedure simultaneously finds the optimal covering factor and optical depth at a given velocity point. Once the optimal combination is found, we derive the formal error of the parameters (see Appendix for full discussion). Our approach is verified by the close match between the resultant flux deviations and the empirical flux errors in both positive and negative directions (see the second figure in the Appendix, Fig. 7).

The errors are not symmetrical. Typically, the "plus" error is larger than the "minus" error, and often much larger. This is due to the exponential dependence of the absorption on the optical depth. For example, if $\tau = 4$, we already absorb 98% of the flux covered by the outflow. Increasing τ by 2 only absorbs an additional 2%. A similar increase in flux requires a decrease of only 0.6 in τ.

In Figure 3, we show the errors associated with the photoionization model presented in Figure 2. O VI has the largest errors because at that velocity its troughs are nearly saturated, and for that reason, the asymmetry in its errors is also most pronounced. H I exhibits the smallest errors and therefore supplies the strongest constraint on the physical solutions for the outflowing gas. The H I errors are the smallest because the observations cover five Lyman series lines, and the intrinsic optical depth ratio of the first three spans a factor of 18. This, coupled with the fact that the Lyβ trough is not close to saturation, yield tight constraints on the column density. In contrast, the intrinsic optical depth ratio between the members of each CNO doublet is 2, yielding significantly less stringent constraints on their N_{ion}. C III is a singlet, and therefore we had to make an assumption regarding its covering fraction. Once we assumed the C III coverage to be the same as C IV, we derived tight constraints on its N_{ion}, since the trough was far from saturation. Finally, a contributing factor for the larger errors of the CNO doublets is that flux errors are associated with both doublet components, while often the difference between the two residual intensities is small compared to the flux values themselves.

We are now in position to ask the first important physical question: do the ion curves in Figure 3 allow for an acceptable solution for the ionization equilibrium for this particular velocity slice of the outflow? That is, is there a combination of N_H and U that will satisfy all the ion-curve constraints? It is evident from Figure 3 that this is not the case, as the error stripes for H I and N V do not overlap on this grid-model plot. A physical solution cannot be obtained for this velocity slice of the outflow, assuming solar abundances. In Figure 4, we show the formal χ^2 solution for the best-fit values of N_H and U for this velocity slice. The reduced $\chi^2 = 5.7$ formally shows that the model does not yield a statistically valid fit for the data. Of the 15 slices, 13 yield reduced χ^2 between 2 and 10, and only two have reduced χ^2 smaller than 2.

3. ABUNDANCE DETERMINATION

3.1. *Method*

The most plausible way to obtain a physical solution for N_H and U in Figure 3 is to drop the assumption of solar abundances. In our parameter-space plots, an increase in abundance is equivalent

to lowering the entire related ion curve, since less $N_{\rm H}$ is needed for the same amount of the said element. We can see from Figure 3 that if the nitrogen abundance is 3 times higher than solar, the N v ion curve will be lower by the same amount and the error stripes for H i and N v will comfortably overlap in parts of the parameter space.

For one velocity slice, we can always achieve a perfect solution (exact crossing of the ion curves) by allowing the CNO abundances relative to hydrogen to be free parameters. Such a solution might be suggestive, but it is considered weak, since we use three free parameters to make the five ion curves cross at the same point. As can be seen in Figure 2, this is always the case. As long as we specify the value of U to be that of the C iii and C iv ion curves' crossing point, the three free abundances parameters allow us to bring all CNO ion curves to meet at that U-value on top of the H i curve.

The way to obtain robust rather than suggestive abundance determinations for the outflow is to use the velocity information. So far we have only dealt with a single velocity slice. It is reasonable to expect that each velocity slice will have an independent ionization solution, i.e., its own $N_{\rm H}$ and U values. The number density and column density of the outflow at each resolution element are determined by the flow's dynamics, which can be quite complicated (Proga 2005). However, it is likely that an outflow component would have the same abundances at all velocities. Therefore, the assumptions we make are that (1) each velocity slice has an independent $N_{\rm H}$, U ionization solution and (2) all velocity slices of the same outflow component have the same chemical abundances.

3.2. *Velocity Coverage*

In Mrk 279, the outflow spans the velocity range -200 to -540 km s^{-1}. As described in Gabel et al. (2005a), the velocity range -300 to -540 km s^{-1} is contaminated by unrelated absorption (probably from the companion galaxy of Mrk 279; see Scott et al. 2004), which is detected in lines from low-ionization species (C ii, C iii, and Si iii) and especially in the H i Lyman series. For this reason, we cannot use the H i trough measurements in the range -300 to -540 km s^{-1} in our ionization and abundance analysis of the flow. We therefore concentrate on the -200 to -300 km s^{-1} range, where we have high-quality uncontaminated measurements for H i, C iii, C iv, N v, and O vi. The *HST*/STIS/E140M grating yields 15 independent resolution elements for this range. We use the N v trough spectrum to fix the velocity points of these elements and interpolate all the other troughs' spectra to that velocity scale. The *FUSE*'s resolution ($\lambda/\Delta\lambda$) is only half that of the STIS/E140M grating, and we interpolated them on the same velocity scale. We used the STIS rather than the *FUSE* resolution for the following reasons: (1) to maintain all the physical information of the STIS troughs; (2) the O vi doublet covered by *FUSE* was the most saturated and yielded the least constraining measurements, and therefore an oversampling by a factor of 2 will not affect the physical conclusion significantly; and (3) the H i measurements arise from one STIS line (Lyα) and two *FUSE* lines (Lyβ and Lyγ), and the derived $N_{\rm H\ I}$ is smooth as a function of velocity (see Fig. 6). Thus, we preserve the STIS velocity resolution for Lyα, while the smoothness of the measurements minimizes the effects of oversampling the *FUSE* data on the physical conclusions, since no structure is seen on small velocity scales.

3.3. *Algorithm*

Using the assumptions detailed in § 3.1, we simultaneously fit all the velocity slices, using methods similar to those used by Gabel et al. (2006). The U and $N_{\rm H}$ associated with each of the 15 velocity bins are the constrained free parameters. All velocity bins have the same given set of CNO abundances relative to H. The abundances are introduced into the fit via a linear scale factor of the metal ionic column densities predicted by the solar metallicity grid of models. This is possible because all the absorbers considered here are optically thin to the EUV ionizing radiation (i.e., the He ii and H i ionization edges are optically thin); thus, the total ionic column densities scale linearly with the abundances of their parent element. After minimizing the χ^2 in each velocity bin, we sum all the minimum values from all the velocity bins. We repeat this process for 11 abundance values for each element (spaced equally in log space), for a total of 11^3 models.

In each velocity bin, there are five measured $N_{\rm ion}$; the summation of these over the 15 velocity bins gives a total of 75 model constraints. The number of free parameters includes two per each velocity bin (U and $N_{\rm H}$) times 15 velocity bins, plus the three CNO abundances: altogether 33 free parameters. The best-fit solution is then the set of velocity-dependent U, $N_{\rm H}$ values, and the C, N, and O abundances that minimize χ^2 from

$$\chi^2 = \sum_i \sum_j \left[\frac{N_{{\rm obs};j,i} - N_{{\rm mod};j}(U, N_{\rm H}) f_j}{\sigma_{j,i}} \right]^2, \qquad (1)$$

where the measured column density of the jth ion in the ith velocity bin $N_{{\rm obs};j,i}$ is compared with the model column densities from the grid $N_{{\rm mod};j}$, f_j is the scale factor relative to solar abundances, and $\sigma_{j,i}$ the measurement uncertainty.

Our initial models sampled a cube of CNO abundance values spanning 0.1–10 times their solar values at a resolution of $\sim$60% between grid points. Upon finding the general location of the best set of CNO abundances, we iteratively refined the span of abundances to a final resolution of 3% between grid points. It is important to verify that we found the absolute rather than a local χ^2 minimum, and to check whether there are other local minima that may give a different but valid abundance solution. For these purposes, we ran additional grid models. In particular, we ran the initial cube model with triple resolution and studied the behavior of χ^2 in that volume. We found no other minima in that phase-space volume.

3.4. *Abundance Results*

The best fit for all 15 velocity slices is obtained using the following set of CNO abundances (relative to solar): C = 2.2, N = 3.5, and O = 1.6. For this model, equation (1) yields $\chi^2 = 47.5$ for 41 degrees of freedom, or a reduced χ^2 of $\chi^2_{\rm red} = 1.16$. In Figure 5, we show the formal χ^2 solution for the best-fit values of $N_{\rm H}$ and U for the single velocity slice shown in Figure 4. The reduced $\chi^2 = 0.8$ formally shows that the model yields a statistically valid fit for the data. A similar situation occurs in most other velocity slices that include the same abundance solution. The range of reduced χ^2 in all velocity slices is 0.5–2.1, for 3 degrees of freedom.

We calculate the model-independent errors associated with these abundance determinations by finding the 90% single-parameter confidence intervals, obtained from changing only the said abundance while keeping the others fixed (following Press et al. [1989] and Taylor [1997]). The results are shown in Table 1. Thus, carbon and oxygen are enhanced by a factor of $\approx$2 relative to solar values, while nitrogen is enhanced by a factor of 3–4, in agreement with the Z^2 scaling indicative of enhanced secondary production in massive stars (Hamman & Ferland 1999, and references therein).

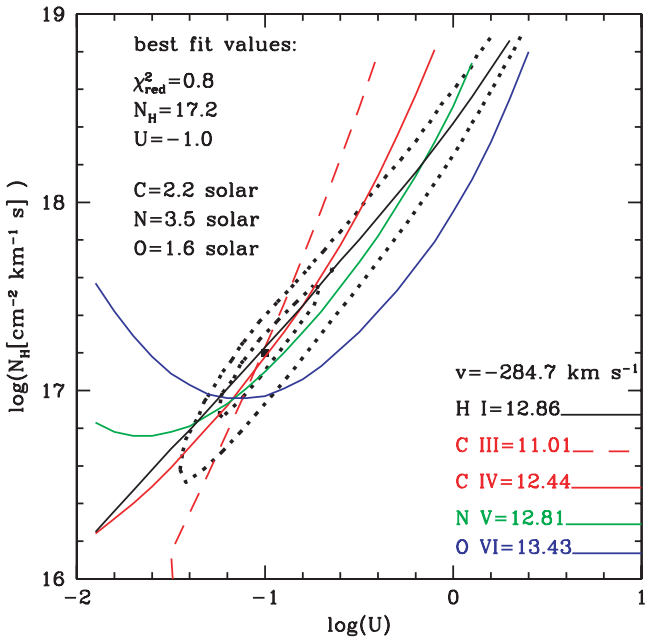

FIG. 5.—Similar to Fig. 4, but for the best global abundance solution. Reduced χ^2 contours are plotted at 5 and 20 for an N_H, U solution (*dotted lines*). Position of the formal solution is marked by the square, and the best-fit values are shown at the top left corner. The best-fit reduced χ^2 gives an acceptable N_H, U solution for this abundance solution.

One can also find a model-dependent error estimate for an assumed Z^2 scaling, since in that model the ratio of C/H and O/H are proportional to each other while N/H $\propto$ (O/H)^2. For this model, the 90% confidence level for nitrogen is only slightly lowered, but the error bars on the oxygen and carbon abundances shrink by 60% and 50%, respectively.

4. AGREEMENT WITH THE X-RAY PHOTOIONIZATION RESULTS

As noted above, we obtained simultaneous X-ray observations (360 ks *Chandra*/LETGS) of the Mrk 279 AGN outflow. The full analysis of the X-ray data is presented by Costantini et al. (2006). Kinematic similarity between the UV and X-ray ionized absorber in this object strongly argues that we are seeing the same outflow in both spectral bands. It is therefore important to compare the independently derived X-ray ionization equilibrium findings with those presented here for the UV data.

Costantini et al. (2006) explored two physical scenarios for the X-ray ionized absorber. The first set of models postulated discrete ionization components, and it was found that a model with two ionization zones gives a good fit to the X-ray absorption data. The second set of models postulated a continuous distribution of the ionization parameter for the absorbing material. Such models were successful in fitting the X-ray absorption data of NGC 5548 (Steenbrugge et al. 2005). Unlike the case for NGC 5548, models with a simple power-law distribution in the ionization parameter did not yield a satisfactory fit to the Mrk 279 *Chandra*/LETGS data. A bimodal distribution was needed for an acceptable fit. Such a model is close in concept to a two ionization zone model. Since the simple two ionization zone model already gives a good fit to the data, we conclude that it provides a more plausible physical description for the Mrk 279 X-ray absorber. We therefore compare our UV results to the results of the two ionization zone X-ray model.

TABLE 1
ABUNDANCES OF THE MRK 279 OUTFLOW RELATIVE TO SOLAR

Element	Abundance
Carbon	2.2 ± 0.7
Nitrogen	3.5 ± 1.1
Oxygen	$1.6^{+0.7}_{-0.8}$

NOTE.—See § 2.3.

For the two ionization component model, Costantini et al. (2006) found the following values (their Table 6):

$$\log(\xi) = 0.47 \pm 0.07 \text{ ergs cm}^{-1},$$
$$N_H = 1.23 \pm 0.23 \times 10^{20} \text{ cm}^{-2}$$

and

$$\log(\xi) = 2.49 \pm 0.07 \text{ ergs cm}^{-1},$$
$$N_H = 3.2 \pm 0.8 \times 10^{20} \text{ cm}^{-2},$$

where the ionization parameter ξ is defined as $\xi \equiv L/n_H r^2$ (L is the luminosity of the source, n_H is the number density of hydrogen in all forms, and r is the distance from the central source). For a given SED, there is a one-to-one correspondence between the ionization parameter ξ and the ionization parameter U, which we are using in this paper. For our Mrk 279 SED, we find $\log(\xi) - \log(U) = 1.5$. Therefore, for the first component, we find $\log(U) = -1.0$. Figure 5 shows the ionization solution for one velocity slice where $\log(U) = -1.0$. This value is representative of all our velocity slices, as we find 90% of the material in this velocity range to have $-1.2 < \log(U) < -0.9$. Thus, the ionization parameter of the low-ionization component deduced from the X-ray analysis is practically identical to the one deduced from the UV analysis. The high-ionization X-ray component does not have any bearing on the UV analysis, since this component is not expected to contribute measurable column density for the UV ions. This is easily verified by inspecting Figure 2. The relative fraction of the UV ions drops dramatically above $\log(U) = -1.0$. Even the fraction of highest ionization UV species (O VI) is lower by more than 2 orders of magnitude for $\log(U) = 1.0$ than for $\log(U) = -1.0$.

How does the total N_H for the low-ionization X-ray component compare with our UV findings? For the velocity range -220 to -300 km s^{-1}, we find from the UV analysis that the total $N_H = 0.8 \times 10^{19}$ cm^{-2}. In order to compare this value to the X-ray determined N_H, two factors have to be taken into account. First, the velocity interval of the UV analysis is only 80 km s^{-1} out of the 340 km s^{-1} of the entire UV trough. It is possible that the rest of the trough has a different amount of N_H per km s^{-1} on average, but in order to get a rough comparison we will simply multiply the above UV derived N_H by 340/80. Second, the X-ray analysis was done assuming solar abundances. Since the UV metallicity enhancement is a factor of 2.4 on average, we need to multiply the UV derived N_H by this additional factor. Accounting for both factors, we find that our rough X-ray equivalent N_H is $N_H = 0.82 \times 10^{20}$ cm^{-2}, which is compatible with the derived value for the low-ionization X-ray component, $N_H = 1.23 \pm 0.23 \times 10^{20}$ cm^{-2}. It is remarkable that the fully independent X-ray and UV ionization solutions agree so well for the Mrk 279 absorber.

Finally, we address the issue of whether our UV derived abundances are compatible with the X-ray analysis. In principle, it is

very difficult to derive absolute abundances from the X-ray data, since there are no hydrogen lines in the X-ray band. Therefore, the X-ray data are insensitive to simple metallicity scaling, and it is not surprising that Costantini et al. (2006) find solar metallicity to be adequate for their models. Barring a handle on the absolute abundances, we look at secondary effects involving ratios of nitrogen to carbon. Our UV findings show that the outflow's N/C = $1.6(\mathrm{N/C})_{\odot}$. The best X-ray measurements are those of C VI and N VI. From Table 5 in Costantini et al. (2006), we find that the modeled C VI is virtually identical to the measured C VI. However, the measured N VI column density $\log (N_{[\mathrm{N\ VI}]})_{\mathrm{obs}} = 16.9 \pm 0.6\ \mathrm{cm}^{-2}$ is higher than the modeled one, $\log (N_{[\mathrm{N\ VI}]})_{\mathrm{model}} = 16.3 \pm 0.36\ \mathrm{cm}^{-2}$ (although the error bars on the two values make them formally consistent with one another). Although the measurements and modeling errors are large, the X-ray data are consistent with a relative enhancement of N/C compared to solar, similar to the one deduced from the UV data. This consistency strengthens our UV abundance findings.

5. DISCUSSION

5.1. *Robustness of the Abundance Determination*

We argue that the work described here is the first reliable abundance determination in AGN outflows. To support this claim, let us review what is necessary for deriving reliable abundances in the outflows, and how well this project met these requirements. In § 5.3, we describe how other previous and current efforts fall short of satisfying these necessary conditions.

Determining the ionization equilibrium and abundances (IEA) in an AGN outflow depends crucially on obtaining reliable measurements of the absorption column densities (N_{ion}) from the observed troughs. As described in the introduction and elsewhere (Arav et al. 1999a, 2001a; de Kool et al. 2001; Gabel et al. 2003; Scott et al. 2004), solving for the velocity-dependent covering fraction is crucial for obtaining reliable N_{ion} from the troughs. Column densities inferred using other techniques (curve of growth, apparent optical depth, and Gaussian modeling) suffer from large systematic uncertainties and many times can only be used as lower limits. We have developed state-of-the-art velocity-dependent methods to determine the covering fraction of both the continuum and BELR, as well as the real optical depth (Gabel et al. 2005a and this work). To implement these methods, a suitable data set must have the following attributes.

1. A spectral resolution larger than 20,000 in order to allow for velocity-dependent analysis across the troughs. *FUSE* and the Echelle gratings on board *HST* give us sufficient resolution.

2. To enable a meaningful covering factor analysis of the CNO doublets, the S/N of the data must be $\gtrsim$20 for the above resolution. The reason for such a high S/N is the need to quantify the differences between the residual intensities of two doublet troughs, which are often only 10%–20% apart (see Gabel 2005a). Very few data sets in the literature achieve this S/N level, since it requires roughly $\gtrsim$15 *HST*/STIS orbits and $\gtrsim$100 ks of *FUSE* exposure time on the brightest AGN outflow targets.

3. The data set must cover troughs from enough ions to be useful for IEA determinations. At the minimum, we need to cover the CNO doublets and three or more of the Lyman series troughs. The latter is a crucial requirement, since abundances cannot be determined without an accurate measurement of H I column density. Only a combination of *FUSE* and *HST* can cover the needed troughs.

4. The troughs associated with different doublet components must be unblended. Otherwise it is impossible to extract covering factors, and the derived N_{ion} are reduced to lower limits. Similarly, the outflow troughs cannot be contaminated with significant Galactic absorption.

5. *FUSE* and *HST*/STIS coverage must be near simultaneous, preferably within the same month. Seyfert outflow troughs are known to show considerable changes over timescales of more than several months (e.g., NGC 3783, Gabel et al. 2005a; Mrk 279, Scott et al. 2004). Any combined analysis of the full data set must rely on no changes in the absorption between the different epochs.

The deep and simultaneous *FUSE* and *HST*/STIS observations of Mrk 279 are the only existing data set that satisfies all these requirements. Therefore, our measurements yield the first sufficient set of reliable N_{ion} to allow for a physical determination of the IEA in AGN outflows.

Our next step was to infer the physical conditions of the absorbing gas using these N_{ion} measurements. Here we introduce an analysis method that uses the full information imprinted on these high-resolution data (Gabel et al. [2006] used similar techniques on the VLT/UVES spectrum of QSO J2233−606). Instead of integrating the N_{ion} across a kinematic component, we treat each resolution element separately.

Physically, this approach is justified, since elements of the flow that are separated by more than several km s^{-1} represent physically separated and sonically disconnected regions. In this way, instead of having constraints on the physical conditions in one kinematic component, we obtain constraints on 15 separate regions. We therefore do not have to use the implicit assumption that the ionization equilibrium is constant across a given component. Working at the spectral resolution of the spectrograph provides the maximum kinematical information without significant scattering between adjacent spectral elements. We also note that these spectrographs have very little instrumental scattered-light components (Howk & Sembach 2000).

We found considerable variation for U and N_{H} over the 15 velocity slices: $-1.4 < \log(U) < -0.9$ and $16.3 < N_{\mathrm{H}} < 17.4$. Thus, it is evident that "classical" kinematic components, which often cover more than 100 km s^{-1}, indeed show significant variation in U and N_{H} as a function of velocity.

For one kinematic component given the set of measured N_{ion}, it is always possible to find a set of CNO abundances that will produce a perfect photoionization solution. It is therefore impossible to assess the physical significance of such a solution. The situation is different for constraining 15 separate regions. We rely on two plausible physical assumptions: that the individual U and N_{H} can vary from one region to another and that the abundances across these regions are constant. This allows us to obtain tight constraints for the individual CNO abundances as described in § 3.4. We spent a great deal of effort to derive physically meaningful errors on our N_{ion} measurements. It is a major achievement that the excellent statistical fit of our abundance model (reduced $\chi^2 = 1.16$) was achieved without any re-adjustments of these errors. This not only validates our methods, but also the physical model we are using to analyze AGN outflows.

5.2. *Possible Caveats*

5.2.1. *Inhomogeneous Absorber Models*

As described above, we invested a large effort in developing and utilizing analysis techniques that solved for two separate covering factors and the optical depth as a function of velocity. An important question in this context is the validity of the assumption of a rigid absorbing-material distribution (essentially a step function), assumed by the partial covering model. Would an inhomogeneous distribution of absorbing material across the emission source (de Kool et al. 2002) yield a good alternative to the partial

covering model? In Arav et al. (2005) we tested inhomogeneous absorber models on the Mrk 279 data set, where the three high-quality Lyα, Lyβ, and Lyγ troughs provided the strongest constraints. We concluded that inhomogeneous absorber models that do not include a sharp edge in the optical depth distribution across the source are not an adequate physical model to explain the trough formation mechanism for the outflow observed in Mrk 279. This result supports the use of partial covering models for AGN outflows.

5.2.2. *SED Uncertainties*

As stated above, the SED we use (see Fig. 1) is arguably the best-determined one for an individual Seyfert study. Nonetheless, we do not cover the crucial 13.6–150 eV ionizing part of the SED, and there is therefore inherent uncertainty that affects the photoionization models. The softest plausible SED is where we connect the last UV point with the first X-ray point (see § 2.2) with a simple power law. This minimizes the assumptions regarding the shape of the unseen portion of the SED, but with the price of assuming a spectral break immediately following the last UV point. We ran photoionization models using such a SED and found that the largest change was a decrease in the carbon abundance by $\sim$10%, with nitrogen and oxygen showing similar but smaller change.

5.3. *Comparison with Other Outflow Metallicity Determinations*

All IEA studies of Seyfert outflows prior to 2003 used $N_{\rm ion}$ measuring techniques that are inadequate for AGN outflow troughs: curve of growth, apparent optical depth, and Gaussian modeling. The key importance of the covering factor was overlooked. Therefore, the IEA findings of these studies suffer from large unquantified systematic errors that can only be corrected to some extent by redoing the analysis using more accurate trough formation models. In many cases, a re-analysis is unwarranted, since one or more of the conditions detailed in § 5.1 is not met: the S/N of the data is insufficient (e.g., Fields et al. 2005), data do not cover troughs from enough ions to be useful for IEA determinations (e.g., Brotherton et al. 2001), doublet troughs are blended (e.g., NGC 4151, Kraemer et al. 2006), there is severe contamination with Galactic absorption (e.g., NGC 3783, Gabel et al. 2003), or *FUSE* and *HST*/STIS coverage is not simultaneous.

A typical recent example is the study of the Mrk 1044 outflow (Fields et al. 2005), which has the following shortcomings. (1) The S/N of the *FUSE* data is too low to allow a covering-factor analysis. (2) There is severe contamination with Galactic absorption in the *FUSE* band, greatly affecting the measurements of the crucial Lyβ trough. (3) *FUSE* and *HST*/STIS observations were taken 6 months apart, allowing significant changes in the absorber to occur, while it is necessary to assume that no absorption change occurred for the sake of the photoionization analysis. (4) There was no attempt to solve for the velocity-dependent covering factor for the STIS observed C IV and N V, which introduces large errors in their $N_{\rm ion}$ determination. (5) The main measured *FUSE* lines (O VI) are totally saturated, and thus the derived O VI column density is only a lower limit. Most importantly, the main conclusion—that the outflow shows a metallicity of at least 5 times solar—is weakened by the fact that the Lyman series troughs are either heavily blended (Lyβ) or of too poor quality (Lyγ) for analysis. A possible increase by a factor of 3 in the H I measurement is reasonable under these conditions and will make the photoionization model (see their Fig. 5) consistent with solar metallicity.

6. SUMMARY

This paper presents a main result of a deep simultaneous UV and X-ray spectroscopic campaign on the AGN outflow seen in Mrk 279, and is the fifth paper resulting from this campaign. Our choice of object combined with the long observations (92 ks with *FUSE*, 16 *HST*/STIS orbits, and 360 ks *Chandra*/LETGS) allowed us to obtain the first reliable determination of chemical abundances in an AGN outflow. We find that relative to solar, the abundances in the Mrk 279 outflow are C $= 2.2 \pm 0.7$, N $= 3.5 \pm 1.1$, and O $= 1.6 \pm 0.8$ (§ 3).

Previous efforts to derive the abundances and ionization equilibrium of the outflows suffered from using inadequate models for the formation of the absorption troughs. Therefore, their inferred ionic column densities are unreliable, and these uncertainties are then amplified by the photoionization models used to deduce the abundances and ionization equilibrium. Much of the problem can be traced to the physical quantities that determine the shape of the observed troughs. In the interstellar medium (ISM) and intergalactic medium (IGM), the shape of absorption troughs singularly depends on the optical depth of the absorbing material. This allows for a straightforward extraction of the all-important ionic column densities. In contrast, AGN outflow absorption troughs are a convolution of velocity-dependent covering factor and optical depth. These two quantities must be deconvolved if one hopes to derive reliable column densities. To accomplish this, a data set must have the following attributes (see § 5.1 for full discussion): a spectral resolution larger than 20,000 and S/N $\gtrsim$ 20 in order to allow for velocity-dependent analysis across the troughs, spectral coverage of at least the CNO doublets and three Lyman series troughs, where the troughs associated with different doublet components must be unblended, and near simultaneous observations of all these troughs.

We chose Mrk 279 because it is by far the best AGN outflow target in satisfying the above requirements. Our deep campaign yielded the necessary high S/N data to do the analysis properly and avoid the many compromising assumptions that plagued previous studies. As a result, we have obtained the best determination of ionization equilibrium to date and the first reliable measurement of abundances in these environments. It is also the first time that the analysis of the UV data is in good agreement with the X-ray analysis. That is, the physical properties of the low-ionization component seen in the X-ray match very well to those we find for the UV gas (see § 4).

In order to extract the physics from the data, we abandoned the old notion of "absorption trough components." This notion is somewhat suitable for ISM and IGM clouds, but is not adequate for studying dynamical absorption structures. Instead, we developed a velocity-dependent analysis technique, which proved crucial in deriving the results of this paper. We believe that these techniques are the only reliable way to determine the physical properties of AGN outflows. This applies to both future UV observations and ground-based Echelle spectroscopy of the outflows.

This study demonstrates that the quality of science that can be achieved by a well-designed campaign is far higher than the combined results of many small projects in this field, providing a strong argument for investing the large resources needed for such studies.

This work is based on observations obtained with *HST* and *FUSE*, both built and operated by NASA. The *FUSE* mission is

operated by the Johns Hopkins University under NASA contract NAS 5-32985. Support for this work was provided by NASA through grants HST-AR-9536 and HST-GO-9688 from the Space Telescope Science Institute, which is operated by the Association of Universities for Research in Astronomy, Inc., under NASA contract NAS 5-26555, through *Chandra* grant 04700532, and by NASA LTSA grant 2001-029. S. R. O. N. is supported financially by NWO, the Netherlands Organization for Scientific Research. We also thank the anonymous referee for useful comments and suggestions.

APPENDIX A

PROFILE FITTING AND IONIC COLUMN DENSITY MEASUREMENTS

In Gabel et al. (2005a, hereafter G05), we performed a detailed global fitting of the intrinsic absorption profiles in the 2003 *FUSE* and STIS spectra of Mrk 279 to derive the velocity-dependent ionic column densities and line-of-sight covering factors. This fitting method allowed for treatment of the individual covering factors of the physically distinct background emission sources, i.e., the continuum source (C_c) and emission-line region (C_l). While the solution from this analysis matched the observed profiles well overall (see Fig. 6 in G05), there were some systematic discrepancies indicating the need for a refinement in the fitting assumptions. Given the crucial importance of having accurate ionic column densities with realistic uncertainties for photoionization modeling of the outflow, we re-address those measurements below.

Two key findings from our global fitting analysis provide the basis for our refined measurements presented here. First, the continuum source was shown to be fully occulted by the outflow, with nonunity effective covering factors due entirely to partial coverage of the emission-line region. We consider this result to be robust: $C_c \approx 1$ was found systematically over the numerous, independently fit velocity bins associated with the highly resolved absorption profiles, and it was found consistently in separate fits to the CNO doublets and the Lyman series lines. It is also geometrically consistent with our understanding of the different size scales of the emission regions, with the UV continuum source much smaller than the BLR.

Second, fits to the C IV and N V doublets deviated slightly but systematically over much of the profiles, with the absorption strength underestimated in the blue and overestimated in the red members of each doublet. This indicates that the effective covering factors for these ions are lower than the global fit solution. In deriving that solution, we assumed all ions share the same covering factors; this was necessary to sufficiently constrain the model so that C_c and C_l could be treated separately. However, with the result that $C_c = 1$, we can now eliminate that simplifying assumption and solve the ionic column densities independently for each doublet pair.

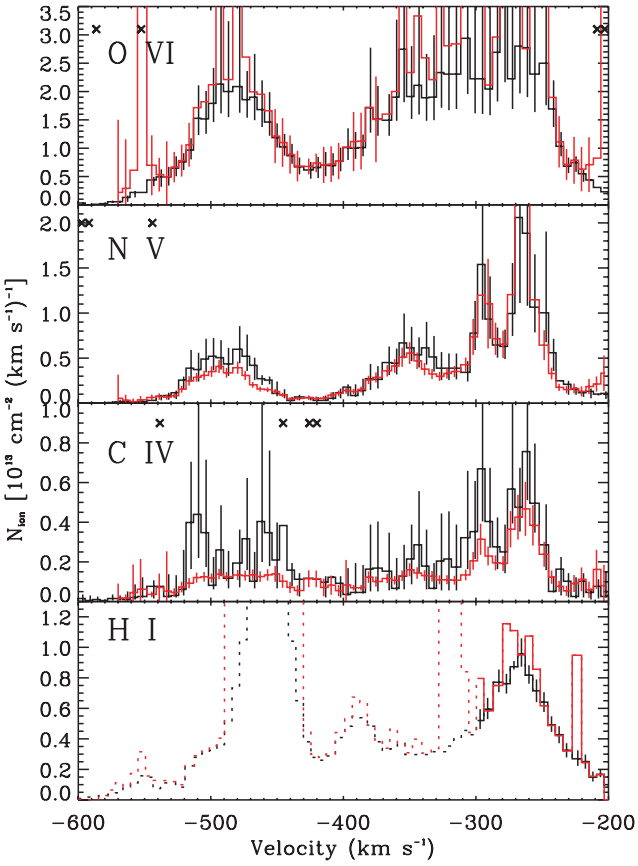

FIG. 6.—Ionic column density profiles derived for the UV outflow in Mrk 279. Results from χ^2 minimization fitting of the absorption profiles, with $C_c = 1$, as described in the text, and associated 1 σ uncertainties are shown with black histograms and error bars. For comparison, the global-fit solutions from G05 are also plotted (*red histograms*). Velocity bins with no valid solution (minimum $\Delta\chi^2 \geq 2$) are denoted with crosses. The region in the H I profile with blended absorption from different physical components, and thus no solution, is plotted with dotted histograms (see G05).

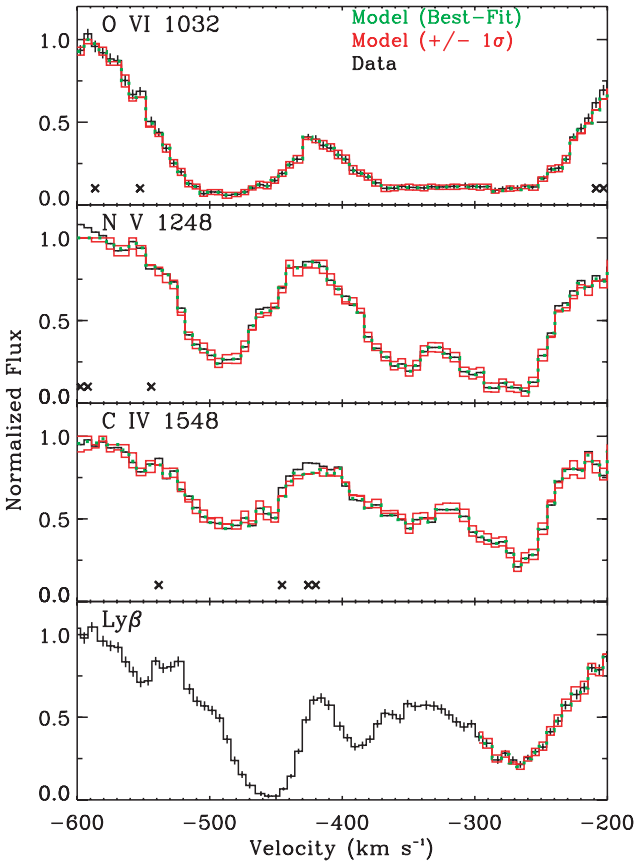

FIG. 7.—Absorption-profile fits and uncertainties compared with the observed spectra. Model profiles corresponding to the best fits to τ and C_l, with $C_c = 1$, are shown in green. Profiles derived using ± 1 σ uncertainties in the fitted parameters are plotted (*red histograms*) for comparison with the 1 σ uncertainties in the fluxes (*black histograms*). Velocity bins with no valid solution are marked with crosses (see G05).

To determine column densities, we used χ^2 fitting analysis, comparing the observed normalized fluxes with the model absorption equation

$$I = 1 + (R_l C_l + R_c C_c)(e^{-\tau} - 1), \tag{A1}$$

where R_l and R_c are the fractional flux contributions of, respectively, the line and continuum emission sources underlying the absorption, and τ is the line optical depth. Equation (A1) comes from the more general expression for an arbitrary number of emission components, given in equation (4) of G05 (see also Ganguly et al. 1999). For each doublet pair, C_l and τ were derived in each velocity bin using equation (1) with $C_c = 1$ by minimizing the $\Delta\chi^2$ function summed over the two doublet lines; the optical depths of the two lines are related by their intrinsic 2 : 1 ratio. The emission-line covering factor was constrained to the physically meaningful range of $0 \leq C_l \leq 1$. Optical depths were converted to ionic column densities using the expression in Savage & Sembach (1991). For 1 σ uncertainties in these parameters, we adopt the maximum offsets from the best-fit values, which give $\chi^2 = 2$ (i.e., equal to the number of lines being fit). For cases of large optical depth (typically $\tau \gtrsim 4$), no upper limit can be determined because of heavy saturation. In these cases, there are only lower limits on the ionic column densities. We measured the H I column density from the Lyman series lines in a similar way. In this case, we fit the combined Lyα, Lyβ, and Lyγ lines, since they all exhibit strong absorption and have the highest signal-to-noise ratio. Since there are three lines in the Lyman fitting, 1 σ uncertainties in the fitted parameters are values giving $\Delta\chi^2 = 3$.

The column density profiles derived from our χ^2 fitting are shown in Figure 6, together with the global fit solutions from G05 for comparison. This shows some important differences that would affect the results of photoionization models. Over much of the profiles, the N V and, especially, C IV column densities are larger than in the global fit, due to the lower effective covering factors associated with these ions. Also, the estimated uncertainties associated with the χ^2 analysis, which we consider to be more realistic as described above, are generally larger. Figure 7 shows the model profiles compared with observed fluxes. Profiles generated using ± 1 σ uncertainties in the parameters (*red histograms*) are seen to match the flux measurement uncertainties (*black error bars*) well overall.

REFERENCES

Allende Prieto, C., Lambert, D. L., & Asplund, M. 2001, ApJ, 556, L63
———. 2002, ApJ, 573, L137
Arav, N. 1997, in ASP Conf. Ser. 128, Mass Ejection from Active Galactic Nuclei, ed. N. Arav, I. Shlosman, & R. J. Weymann (San Francisco: ASP), 208
Arav, N., Becker, R. H., Laurent-Muehleisen, S. A., Gregg, M. D., White, R. L., Brotherton, M. S., & de Kool, M. 1999a, ApJ, 524, 566
Arav, N., Brotherton, M. S., Becker, R. H., Gregg, M. D., White, R. L., Price, T., & Hack, W. 2001a, ApJ, 546, 140

Arav, N., Kaastra, J., Kriss, G. A., Korista, T. K., Gabel, J., & Proga, D. 2005, ApJ, 620, 665
Arav, N., Kaastra, J., Steenbrugge, K., Brinkman, B., Edelson, R., Korista, T. K., & de Kool, M. 2003, ApJ, 590, 174
Arav, N., Korista, K. T., de Kool, M. 2002, ApJ, 566, 699
Arav, N., Korista, K. T., de Kool, M., Junkkarinen, V. T., & Begelman, M. C. 1999b, ApJ, 516, 27
Arav, N., Li, Z. Y., & Begelman, M. C. 1994, ApJ, 432, 62
Arav, N., et al. 2001b, ApJ, 561, 118
Baldwin, J. A., & Netzer, H. 1978, ApJ, 226, 1
Barlow, T. A., Hamann, F., & Sargent, W. L. W. 1997, in ASP Conf. Ser. 128, Mass Ejection from Active Galactic Nuclei, ed. N. Arav, I. Shlosman, & R. J. Weymann (San Francisco: ASP), 13
Brotherton, M. S., Green, R. F., Kriss, G. A., Oegerle, W., Kaiser, M. E., Zheng, W., Hutchings, J. B. 2002, ApJ, 565, 800
Churchill, C. W., Schneider, D. P., Schmidt, M., & Gunn, J. E. 1999, AJ, 117, 2573
Costantini, E., et al. 2007, A&A, 461, 121
Crenshaw, D. M., Kraemer, S. B., Boggess, A., Maran, S. P., Mushotzky, R. F., & Wu, C. C. 1999, ApJ, 516, 750
de Kool, M., Arav, N., Becker, R. H., Laurent-Muehleisen, S. A., White, R. L., Price, T., & Gregg, M. D. 2001, ApJ, 548, 609
de Kool, M., Korista, K. T., & Arav, N. 2002, ApJ, 580, 54
Dietrich, M., Appenzeller, I., Hamann, F., Heidt, J., Jäger, K., Vestergaard, M., & Wagner, S. J. 2003, A&A, 398, 891
Dietrich, M., Wagner, S. J., Courvoisier, T. J.-L., Bock, H., & North, P. 1999, A&A, 351, 31
Fan, X., et al. 2004, AJ, 128, 515
Ferland, G. J., Baldwin, J. A., Korista, K. T., Hamann, F., Carswell, R. F., Phillips, M., Wilkes, B., & Williams, R. E. 1996, ApJ, 461, 683
Ferland, G. J., Korista, K. T., Verner, D. A., Ferguson, J. W., Kingdon, J. B., & Verner, E. M. 1998, PASP, 110, 761
Fields, D. L., Mathur, S., Pogge, R. W., Nicastro, F., Komossa, S., & Krongold, Y. 2005, ApJ, 634, 928
Gabel, J. R., Arav, N., & Kim, T.-S. 2006, ApJ, 646, 742
Gabel, J. R., et al. 2003, ApJ, 583, 178
———. 2005a, ApJ, 623, 85 (G05)
———. 2005b, ApJ, 631, 741
Ganguly, R., Eracleous, M. C., Charlton, J. C., & Churchill, C. W. 1999, AJ, 117, 2594
Hamann, F., 1997, ApJS, 109, 279
Hamann, F., Barlow, T. A., Junkkarinen, V., & Burbidge, E. M. 1997, ApJ, 478, 80
Hamann, F., & Ferland, G. 1992, ApJ, 391, L53
———. 1999, ARA&A, 37, 487
Holweger, H. 2001, in AIP Conf. Proc. 598, Solar and Galactic Composition: A Joint SOHO/ACE Workshop , ed. R. F. Wimmer-Schweingruber (New York: AIP), 23
Howk, J. C., & Sembach, K. R. 2000, AJ, 119, 2481
Hwang, C. Y., & Bowyer, S. 1997, ApJ, 475, 552
Kaastra, J. S., Mewe, R., Liedahl, D. A., Komossa, S., & Brinkman, A. C. 2000, A&A, 354, L83
Kaastra, J. S., Steenbrugge, K. C., Raassen, A. J., van der Meer, R., Brinkman, A. C., Liedahl, D. A., Behar, E., & de Rosa, A. 2002, A&A, 386, 427
Kaspi, S., Brandt, W. N., Netzer, H., Sambruna, R., Chartas, G., Garmire, G. P., & Nousek, J. A. 2000, ApJ, 535, L17
Kaspi, S., Maoz, D., Netzer, H., Peterson, B. M., Vestergaard, M., & Jannuzi, T. 2005, ApJ, 629, 61
Kaspi, S., et al. 2002, ApJ, 574, 643
Korista, T. K., Voit, G. M., Morris, S. L., & Weymann, R. J. 1993, ApJS, 88, 357
Kraemer, S. B., et al. 2006, ApJS, 167, 161
Kriss, G. A., et al. 2000, ApJ, 538, L17
Nagao, T., Marconi, A., & Maiolino, R. 2006, A&A, 447, 157
Netzer, H. 1990, in Active Galactic Nuclei, ed. R. D. Blandford, H. Netzer, L. Woltjer, T. J.-L. Courvoisier, & M. Mayor (New York: Springer), 57
Pettini, M., Rix, S. A., Steidel, C. C., Adelberger, K. L., Hunt, M. P., & Shapley, A. E. 2002, ApJ, 569, 742
Press, W. H., Flannery, B. P., Teukolsky, S. A., & Vetterling, W. T. 1989, Numerical Recipes in Pascal: The Art of Scientific Computing (Cambridge: Cambridge Univ. Press)
Proga, D. 2005, ApJ, 630, L9
Savage, B. D., & Sembach, K. R. 1991, ApJ, 379, 245
Scott, J. E., et al. 2004, ApJS, 152, 1
Shields, G. A. 1976, ApJ, 204, 330
Steenbrugge, K. C., et al. 2005, A&A, 434, 569
Taylor, J. 1997, Introduction to Error Analysis: The Study of Uncertainties in Physical Measurements (2nd ed.; New York: Univ. Science Books)
Telfer, R. C., Kriss, G. A., Zheng, W., Davidson, A. F., & Green, R. F. 1998, ApJ, 509, 132
Weymann, R. J., Morris, S. L., Foltz, C. B., & Hewett, P. C. 1991, ApJ, 373, 23
Weymann, R. J., Turnshek, D. A., & Christiansen, W. A. 1985, in Astrophysics of Active Galaxies and Quasi-stellar Objects (Mill Valley: Univ. Science Books), 333